Nano Research
2022, 15(12): 10037–10043

ISSN 1998-0124 CN 11-5974/O4
https://doi.org/10.1007/s12274-022-4376-5

Research Article

Pd single-atom catalysts derived from strong metal–support interaction for selective hydrogenation of acetylene

Yalin Guo[1,2], Yangyang Li[1,2], Xiaorui Du[3], Lin Li[1], Qike Jiang[4] (✉), and Botao Qiao[1] (✉)

[1] *CAS Key Laboratory of Science and Technology on Applied Catalysis, Dalian Institute of Chemical Physics, Chinese Academy of Sciences, Dalian 116023, China*
[2] *University of Chinese Academy of Sciences, Beijing 100049, China*
[3] *Guangzhou Institute of Energy Conversion, Chinese Academy of Sciences, Guangzhou 510640, China*
[4] *Dalian National Laboratory for Clean Energy, Dalian Institute of Chemical Physics, Chinese Academy of Sciences, Dalian 116023, China*

Received: 19 February 2022 / **Revised:** 28 March 2022 / **Accepted:** 29 March 2022

ABSTRACT

Selective hydrogenation of acetylene in excess ethylene is an important reaction in both fundamental study and practical application. Pd-based catalysts with high intrinsic activity are commonly employed, but usually suffer from low selectivity. Pd single-atom catalysts (SACs) usually exhibit outstanding ethylene selectivity due to the weak π-bonding ethylene adsorption. However, the preparation of high-loading and stable Pd SACs is still confronted with a great challenge. In this work, we report a simple strategy to fabricate Pd SACs by means of reducing conventional supported Pd catalysts at suitable temperatures to selectively encapsulate the co-existed Pd nanoparticles (NPs)/clusters. This is based on our new finding that single atoms only manifest strong metal–support interaction (SMSI) at higher reduction temperature than that of NPs/clusters. The derived Pd SACs (Pd_1/CeO_2 and Pd_1/α-Fe_2O_3) were applied to acetylene selective hydrogenation, exhibiting much improved ethylene selectivity and high stability. This work offers a promising way to develop stable Pd SACs easily.

KEYWORDS

selective hydrogenation of acetylene, Pd single-atom catalysts (SACs), weak π-bonding ethylene adsorption, strong metal–support interaction (SMSI)

1 Introduction

Selective hydrogenation of acetylene in excess ethylene is an important industrial reaction to remove trace acetylene impurities in ethylene feed [1–3]. Supported Pd-based catalysts have been extensively studied and industrially used for decades due to their high intrinsic activity. However, the low selectivity, especially at full acetylene conversion, has been a long-standing issue that needs to be addressed. To improve ethylene selectivity, Pd active sites are usually selectively poisoned [2, 4, 5] or diluted by another metal to form Pd-M alloy/intermetallic compounds [6–16] in industry. These strategies are certainly helpful to improve selectivity but often at the cost of activity because substantial amount of Pd is blocked by the poisonous substance or diluting metals.

Recently, single-atom catalysts (SACs) have attracted widespread attention in heterogeneous catalysis field because of their superior activity and maximized metal atom utilization efficiency [17–23]. Supported Pd SACs have shown outstanding hydrogenation selectivity on account of the isolation nature of supported metals [24, 25]. However, synthesizing stable and high-loading Pd-based SACs, especially on oxide supports, still remains a grand challenge. So far, only few examples regarding the synthesis and application of Pd SACs with relatively high metal loadings have been reported [26–29]. In addition, the stability of SACs under reductive atmosphere is also a bottleneck in practical application.

Strong metal–support interaction (SMSI), a phenomenon that reducible oxides supported Pt-group metals will lose their capability to adsorb small molecules such as CO and H_2 after high-temperature reduction, has been intensively studied over 40 years [30–38]. With recent discoveries on various new types of SMSI as well as new characteristics of SMSI, this topic has attracted renewed attention [38–50]. Recently, we have revealed that Pt_1/TiO_2 SACs can manifest classical SMSI but at a much higher reduction temperature than that for Pt nanoparticles (NPs), and the suppression of CO adsorption on Pt single atoms stems from coordination saturation distinguished from the physical coverage of Pt NPs by the support [51]. This finding offers a new strategy to fabricate stable SACs with improved catalytic performance, especially the optimized selectivity, by simply manipulating reduction temperatures to control different support encapsulation degrees.

Herein, we demonstrated that this strategy can be extended to fabricate stable Pd SACs (Pd_1/CeO_2 SAC and Pd_1/α-Fe_2O_3) via high-temperature reduction treatment of the corresponding supported Pd catalysts prepared by common adsorption method. The constructed Pd SACs show not only good stability but also dramatically improved ethylene selectivity due to the weak π-bonding adsorption of ethylene.

Address correspondence to Qike Jiang, qike@dicp.ac.cn; Botao Qiao, bqiao@dicp.ac.cn

2 Methods

2.1 Preparation

2.1.1 Chemicals

Cerium nitrate ($Ce(NO_3)_3·6H_2O$), ferric nitrate ($Fe(NO_3)_3·9H_2O$), sodium carbonate (Na_2CO_3), and tetraamminepalladium(II) nitrate solution ($Pd(NO_3)_2·4NH_3$, 10 wt.% in H_2O) were all purchased from Sigma-Aldrich. All reagents were analysis reagent (A.R.) and were used without further purification. Deionized water was obtained from a Millipore Autopure system.

2.1.2 Synthesis of support (CeO_2 and α-Fe_2O_3)

CeO_2 and α-Fe_2O_3 supports were synthesized by a co-precipitation method. In detail, $Ce(NO_3)_3·6H_2O$ (1 mol/L) or $Fe(NO_3)_3·9H_2O$ (1 mol/L) aqueous solution was added drop-wise into an aqueous solution of Na_2CO_3 (1 mol/L) under stirring with the final pH of the solution being controlled at approximately 8. After being stirred continuously and aged for 3 h, respectively, the resulting precipitate was filtered and washed with distilled water. The recovered solid was dried at 60 °C overnight and then calcined at 400 °C for 5 h, forming CeO_2 or α-Fe_2O_3 support [40, 52].

2.1.3 Synthesis of 1 wt.% Pd/CeO_2 and 1 wt.% Pd/α-Fe_2O_3

The Pd species was introduced onto the support by a facile adsorption method. In a typical preparation process, 1 g support (CeO_2 or α-Fe_2O_3) powder was dispersed in 50 mL deionized water with rigorous stirring. 0.27 mL of 10 wt.% $Pd(NO_3)_2·4NH_3$ in H_2O was added drop-wise into support suspension liquid under stirring. After stirring for 4 h followed by aging for 2 h, the solution was filtered and washed with deionized water. Then the recovered solid was dried at 60 °C overnight and calcined at 400 °C for 5 h. The synthesized catalysts were denoted as Pd/CeO_2 and Pd/α-Fe_2O_3. Pd/CeO_2 was followed by reduction under 10 vol.% H_2/He at 200, 500, and 600 °C, denoted as Pd/CeO_2-200H, Pd/CeO_2-500H, and Pd/CeO_2-600H, respectively. The Pd/CeO_2-600H catalyst was re-oxidized under 20 vol.% O_2/He at 500 °C, denoted as Pd/CeO_2-600H-O500. Similarly, Pd/α-Fe_2O_3 was reduced and denoted as Pd/α-Fe_2O_3-200H, Pd/α-Fe_2O_3-400H, and Pd/α-Fe_2O_3-500H, respectively. And the Pd/α-Fe_2O_3-500H was re-oxidized, denoted as Pd/α-Fe_2O_3-500H-O500.

2.2 Characterization

Inductively coupled plasma optical emission spectrometer (ICP-OES): The actual Pd loadings of all catalysts were determined by ICP-OES on ICPS-8100 instrument (Shimadzu Co., Ltd.).

X-ray diffraction (XRD): Powder XRD was performed at a PANalytical X'Pert PRO X-ray diffractometer using Cu-Kα radiation (λ = 0.15432 nm), operating at 40 kV and 40 mA.

Aberration-corrected scanning transmission electron microscopy (AC-STEM), electron energy loss spectroscopy (EELS), and energy disperse X-ray spectroscopy (EDS): The AC-STEM, EDS, and EELS were obtained on JEOL JEM-ARM200F operated at 200 kV equipped with a Gatan Quantum 965 image filter system. The chemical compositions of the covering layer of Pd NPs were characterized by directly putting electron beam at the Pd NPs in a STEM mode. Before measurements, the samples were ultrasonically dispersed in ethanol, and then a drop of the solution was put onto the carbon film supported by a copper grid.

Diffuse reflectance infrared Fourier transform spectroscopy (DRIFTS): *In situ* DRIFTS was acquired with a VERTEX 70 V infrared spectrometer equipped with a mercury cadmium telluride (MCT) detector and operated at a resolution of 4 cm^{-1} using 32 scans. Before CO adsorption, all catalysts were purged with pure He for 30 min at 200 °C after corresponding treatments (reduction or re-oxidation). After cooled to room temperature, the background spectrum was recorded and then 5 vol.% CO/He was introduced into the reaction cell, and the spectra were collected until the state steady. Subsequently, pure He was introduced again to remove the gas phase CO, and the spectra were also recorded.

X-ray photoelectron spectroscopy (XPS): XPS characterization was conducted on an X-ray photoelectron spectrometer (USA, ThermoFischer, ESCALAB 250Xi) equipped with Al Kα excitation source (1,486.8 eV) and with C as the internal standard (C 1s = 284.8 eV).

Thermogravimetric analysis (TGA): TGA was conducted on a synchronous thermal analyzer (STA 449 F3). The catalysts were heated to 150 °C in O_2 flow with a ramp rate of 5 °C/min and maintained at this temperature for 0.5 h to remove H_2O, then further heated to 800 °C with same ramp rate, recording the data of weight.

2.3 Evaluation of selective hydrogenation of acetylene in excess ethylene

Acetylene selective hydrogenation in excess ethylene over different catalysts was evaluated in a quartz fixed-bed flow reactor (d = 10 mm) with 20 mg catalysts and 200 mg quartz sand diluted. The as-prepared catalysts were reduced in H_2 (10 vol.% H_2/He, 30 mL/min) at different reduction temperatures prior to the hydrogenation reaction. After being cooled to room temperature, feed gas of 2 vol.% C_2H_2, 20 vol.% H_2, 40 vol.% C_2H_4, and balance He (30 mL/min) was introduced to the fixed-bed reactor followed by temperature programmed testing. Gas composition at the inlet and outlet was analyzed by online GC (A91) equipped with a flame ionization detector (FID) and a PORAPAK-N column with helium as the carrier gas. In our tests, C_2H_4 and C_2H_6 were the only C_2 products and the formation of oligomers was negligible, most probably due to the basic property of CeO_2 and α-Fe_2O_3 supports. The conversion of acetylene and the selectivity to ethylene were calculated as the following

$$\text{Conversion} = \frac{C_2H_2(\text{feed}) - C_2H_2}{C_2H_2(\text{feed})} \times 100\% \quad (1)$$

$$\text{Selectivity} = \left(1 - \frac{C_2H_6 - C_2H_6(\text{feed})}{C_2H_2(\text{feed}) - C_2H_2}\right) \times 100\% \quad (2)$$

where C_2H_2(feed) means the concentration of C_2H_2 in feed gas, C_2H_2 means the concentration of C_2H_2 after reaction, C_2H_6(feed) means the concentration of C_2H_6 in feed gas, which is usually nearly 0, and C_2H_6 means the concentration of C_2H_6 after reaction.

3 Results and discussion

The actual Pd loading on Pd/CeO_2 was measured to be 0.98 wt.%, almost same to the nominal one, suggesting no Pd loss occurred during catalyst preparation. The XRD patterns of the synthesized CeO_2 and Pd/CeO_2 are presented (Fig. S1 in the Electronic Supplementary Material (ESM)). Only diffraction peaks of CeO_2 are observed but diffraction pattern associated with Pd species is invisible, indicating a high dispersion of Pd species on Pd/CeO_2. This was confirmed by the AC-STEM images and EDS analysis (Fig. S2 in the ESM), which shows the absence of Pd NPs on Pd/CeO_2-200H. Therefore, the Pd must be existed as highly dispersed Pd small clusters and/or singly dispersed Pd atoms which are hardly distinguished by AC-STEM due to the low Z-contrast of Pd and Ce. But according to the DRIFTS results and catalytic performance (we will discuss this later), we can safely

claim that both are presented. After reduction at 600 °C, Pd/CeO_2-600H shows a mean Pd NP size of 2.8 nm (Fig. S3 in the ESM), suggesting some Pd clusters and single atoms sintered upon reduction. This is as expected due to the usually low stability of SACs in reduction atmosphere. Pd single atoms are still presented (see DRIFTS results later) but indiscernible on AC-STEM images due to the low contrast [52–54].

One of the typical characteristics of classical SMSI is the mass transport from support. On Pd/CeO_2-600H the encapsulation layer can be observed in bright filed (BF) images (Fig. 1(a)), and the composition is CeO_x confirmed by high-angle annular dark-field (HAADF)-STEM and EELS (Figs. 1(b) and 1(e)). Another characteristic of classical SMSI is that the encapsulation layer will retreat after oxidation treatment, i.e., encapsulation layer is reversible under opposite treatment condition. We therefore examined the Pd/CeO_2-600H sample after oxidation treatment at 500 °C. Pd/CeO_2-600H-O500 shows an obvious but not complete retreat of the CeO_x cover layer as confirmed by both BF-STEM image (Fig. 1(c)) and the weakened EELS signal of Ce (Figs. 1(d) and 1(e)), consistent well with the previous reports [33, 55–57]. Significantly, the Pd NPs became small with a mean size of 1.8 nm (Fig. S4 in the ESM), suggesting a re-dispersion of Pd upon the oxidation treatment [58–60].

DRIFTS of CO absorption (CO-DRIFTS) is one of the most powerful techniques applied to the characterization of SMSI owing to its sensitivity to probe both adsorption property and electronic structure of catalysts. Adsorption suppression of small molecules, electron transfer and the reversibility of above phenomena are all discernible via CO-DRIFTS. We therefore performed CO-DRIFTS to further verify SMSI of this set of catalysts and the results are presented (Fig. 2).

For Pd/CeO_2 reduction at 200 °C (Pd/CeO_2-200H), besides gaseous CO (2,173 cm^{-1} for R-branch and 2,120 cm^{-1} for P-branch), a strong peak centred at 2,080 cm^{-1} and a broad band existing in the range of 1,800–1,990 cm^{-1} are observed. The former is ascribed to linear CO adsorption on Pd NPs while the latter is the bridged and/or three-hollowed CO adsorption [61]. The linear CO adsorption on Pd single atoms is, unfortunately, overlapped with the P-branch of gaseous CO [62]. In addition, the linear CO adsorption on Pd is too weak to be distinguished from gaseous CO by simple He purge because linear CO adsorption will desorb as well. However, by adjusting the CO inflow and desorption rate, CO-DRIFTS spectra on Pd/CeO_2-200H show an obvious linear CO adsorption on single Pd atoms at 2,133 cm^{-1} (Fig. S5 in the ESM), suggesting the co-existence of Pd single atoms and NPs/clusters. After reduction at 600 °C, both linear and bridged CO adsorption on Pd NPs disappeared, suggesting the complete encapsulation of Pd NPs by support. On the contrary, after He purge for 0.5 and 1 min, the linear CO adsorption on Pd single atoms can be observed clearly which is shifted to a lower frequency (2,107 cm^{-1}) compared with that on Pd/CeO_2-200H. This assignment can be confirmed by the weaker adsorption and no frequency shift with CO coverage upon purge, in contrast to the stronger CO adsorption and frequency shift with CO coverage change on Pd NPs (from 2,080 to 2,070 cm^{-1}). The lower frequency must have originated from a lower chemical state of Pd single atoms after high-temperature reduction. The DRIFTS results and AC-STEM images verify the co-existence of Pd single atoms and NPs on both Pd/CeO_2-200H and Pd/CeO_2-600H. The presence of CO adsorption on Pd single atoms whilst absence of CO adsorption on Pd NPs after reduction at 600 °C stresses that the occurrence of SMSI on Pd NPs is easier than that on single atoms [51]. After calcination at 500 °C under O_2 for re-oxidation treatment (Pd/CeO_2-600H-O500), all CO adsorption peaks on Pd NPs appear again while the peak positions are slightly blue-shifted and intensity is weakened compared with that on Pd/CeO_2-200H, implying the electron transport between metal Pd and support CeO_2 and the encapsulation is not totally recovered in consistent with the STEM characterization results.

XPS was also performed to verify the reversible electron transfer between metal and support during the reduction and re-oxidation processes for SMSI (Fig. 3). The Pd species with a binding energy of 337.8 eV on Pd/CeO_2 can be attributed to the $Pd^{\delta+}$ ($2 < \delta \leq 4$) in the form of $Pd_xCe_{1-x}O_2$ at the interfaces [63–66]. The binding energies of Pd 3d decrease to 335 and 337 eV after reduction at 600 °C, which are assigned to a mixture of Pd^0 in the metal state

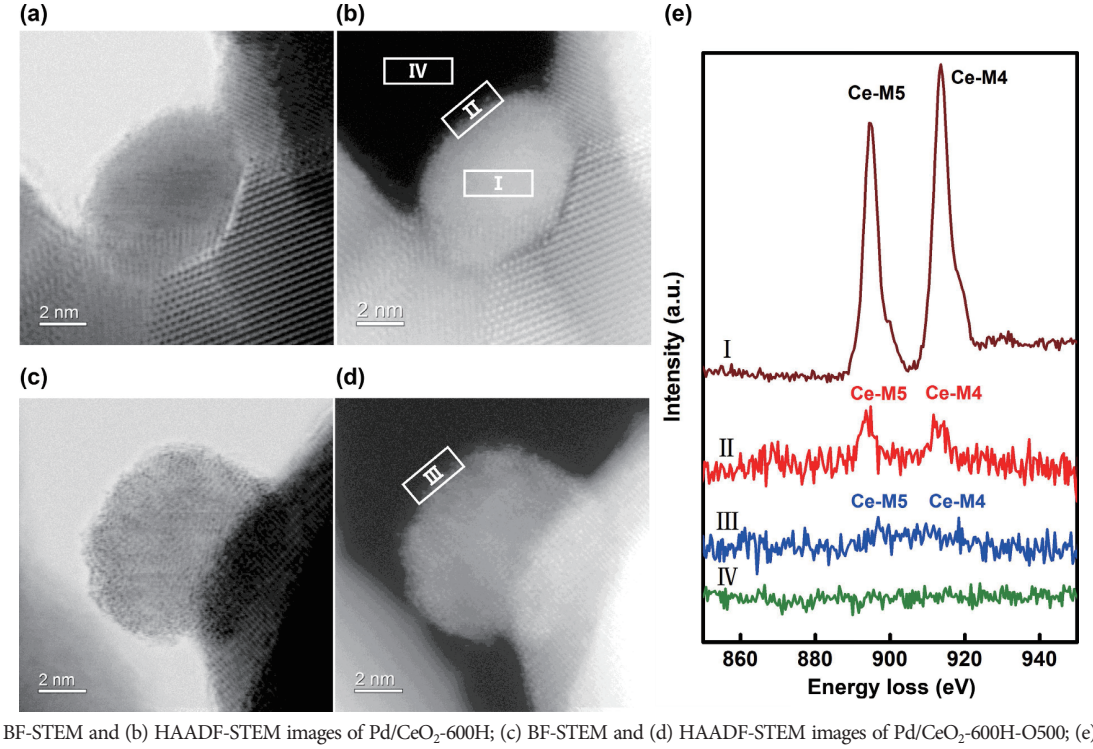

Figure 1 (a) BF-STEM and (b) HAADF-STEM images of Pd/CeO_2-600H; (c) BF-STEM and (d) HAADF-STEM images of Pd/CeO_2-600H-O500; (e) EELS spectra of Pd/CeO_2-600H and Pd/CeO_2-600H-O500.

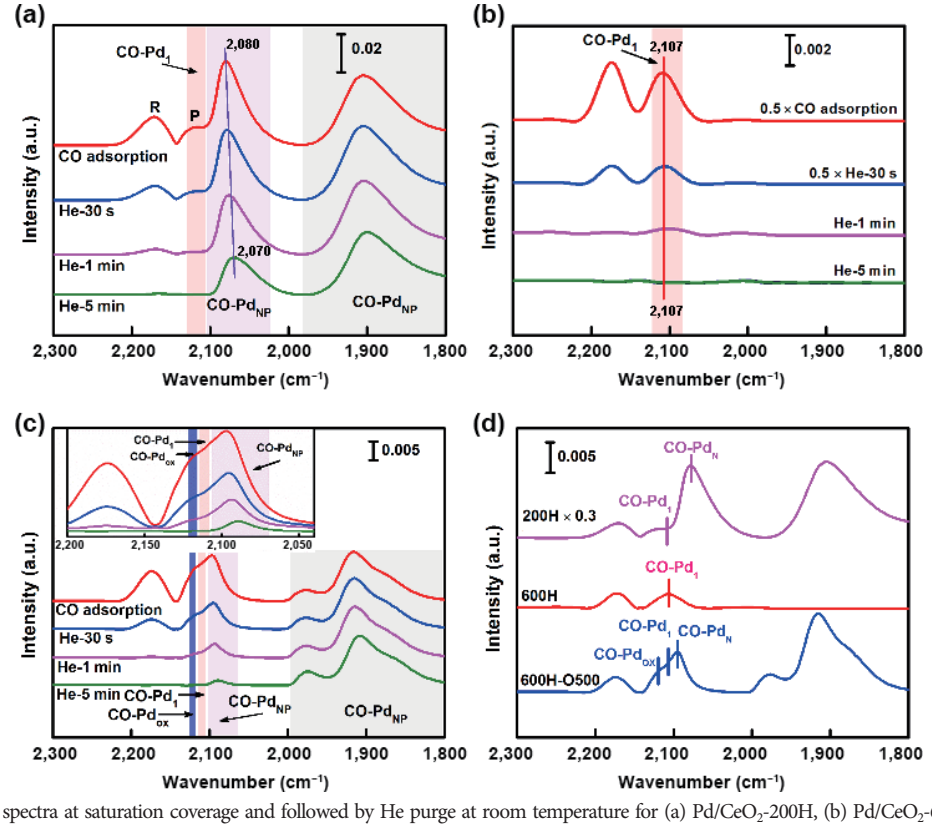

Figure 2 CO-DRIFTS spectra at saturation coverage and followed by He purge at room temperature for (a) Pd/CeO_2-200H, (b) Pd/CeO_2-600H, and (c) Pd/CeO_2-600H-O500; and (d) He purging of above three catalysts for the same time.

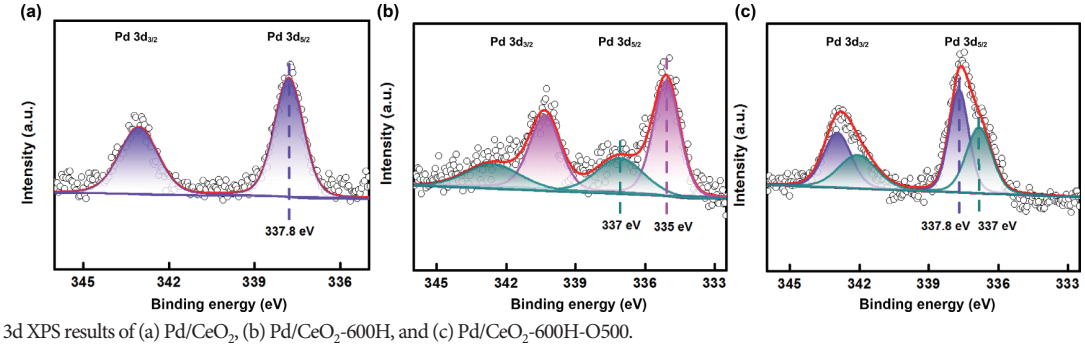

Figure 3 Pd 3d XPS results of (a) Pd/CeO_2, (b) Pd/CeO_2-600H, and (c) Pd/CeO_2-600H-O500.

and $Pd^{\delta+}$ in the form of PdO_x [67], suggesting the presence of Pd single atoms and electron transfer from the CeO_2 support to Pd species. Subsequently, the binding energies shift to 337 and 337.8 eV after re-oxidation, respectively, which can be explained by only partial electron transfer recovered in agreement with the CO-DRIFTS results.

Above characterization results demonstrated that the occurrence of SMSI on Pd NPs is easier than that on Pd single atoms, and the physical coverage of NPs by support is the main origin for the suppression of small molecules adsorption. Thus, Pd_1/CeO_2 SAC can be obtained from modifying common CeO_2 supported Pd catalysts by controlling the SMSI state, i.e., selectively encapsulating Pd NPs while exposing Pd single atoms. Selective hydrogenation of acetylene in excess ethylene is of great importance in both fundamental study and practical application, and the ethylene selectivity is very sensitive to the isolation or aggregation nature of Pd atoms [24]. Therefore, we can expect an improved selectivity by manipulating the SMSI state.

The reaction was conducted below 200 °C for all samples at a weight hourly space velocity (WHSV) of 90,000 mL/(h·g_{cat}) (Fig. 4). Pd/CeO_2-200H exhibits high activity with a full conversion at 80 °C but truly low selectivity (−900%), which means not only the overhydrogenation of acetylene but also direct hydrogenation of raw ethylene occurred. After reduction at a higher temperature (500 °C), the Pd NPs are partially encapsulated and the selectivity dramatically increases from −900% to −50%, despite the activity decreases correspondingly. However, for Pd/CeO_2-500H, overhydrogenation and direct ethylene hydrogenation are still existent. Further raising reduction temperature to 600 °C, the Pd NPs are completely encapsulated while Pd single atoms exposed as confirmed by the CO-DRIFTS results (Figs. 2(b) and 2(d)). Acetylene is fully transformed at 160 °C and the selectivity enhances significantly to 85%, which outperforms many previously reported Pd-based catalysts [12, 68–71]. Javier Pérez-Ramírez has reported that CeO_2 itself is active for semi-hydrogenation reaction [72]. However, a control experiment shows that in our condition the CeO_2 support reduced at 600 °C (CeO_2-600H) is barely active, illuminating the reactivity comes from isolated Pd active sites rather than reduced CeO_2 support. Isolation nature of the Pd species is in favour of weak π-bonding adsorption for ethylene, leading to a much higher ethylene selectivity. It is emphasized that the SMSI effect guarantees the catalyst stability via strong interaction which inhibits aggregation for Pd atoms after high-temperature reduction.

It was demonstrated that SMSI effect is universal and can be extended to other reducible oxide supports such as FeO_x, MnO,

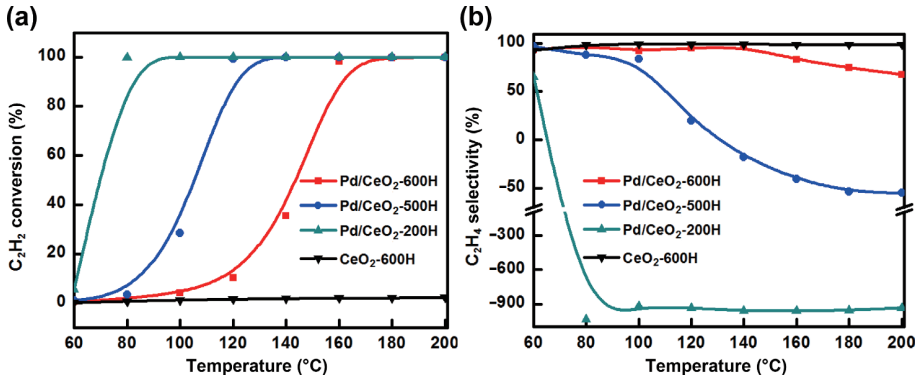

Figure 4 Catalytic performance of Pd/CeO_2 serial catalysts. (a) Acetylene conversion and (b) ethylene selectivity as a function of temperature for selective hydrogenation of acetylene in excess ethylene over CeO_2-600H, Pd/CeO_2-200H, Pd/CeO_2-500H, and Pd/CeO_2-600H. Reaction conditions: 2 vol.% C_2H_2, 20 vol.% H_2, and 40 vol.% C_2H_4 balanced with He; WHSV = 90,000 mL/(h·g_{cat}).

and V_2O_3 [55, 73]. We therefore speculated that Pd SACs could also be constructed on other reducible oxide supports, by selectively encapsulating the co-existed NPs and exposing Pd single atoms, to distinctly refine the catalytic performance. To verify the universality, we further prepared Pd/α-Fe_2O_3 catalyst by same method with an actual Pd loading of 0.31 wt.% determined by ICP-OES. Similarly, XRD measurement suggests no Pd diffraction pattern was observed (Fig. S6 in the ESM). AC-STEM and EDS images show no Pd NPs present on Pd/α-Fe_2O_3, which implies the high dispersion (Fig. S7 in the ESM). After low temperature reduction, for Pd/α-Fe_2O_3-200H, the highly dispersed Pd species is partly aggregated to Pd NPs, on which Pd single atoms and NPs are co-existent (Fig. S8 in the ESM). After high temperature reduction and re-oxidation, for Pd/α-Fe_2O_3-500H and Pd/α-Fe_2O_3-500H-O500, Pd species still exists in the form of Pd single atoms and NPs (Fig. S9 in the ESM). AC-STEM and EELS images show the reversible encapsulation of Pd NPs by supporting FeO_x after reduction at 500 °C and re-oxidation treatment (Fig. S10 in the ESM). Electron transfer between Pd species and α-Fe_2O_3 was manifested by XPS results (Fig. S11 in the ESM). The positive valence of Pd 3d after deeper reduction at 500 °C is attributed to single atoms over Pd/α-Fe_2O_3-500H. Based on above results, Pd/α-Fe_2O_3 catalysts pretreated with different reduction temperatures were applied to selective hydrogenation of acetylene. Remarkably, same scenario to Pd/CeO_2 catalysts was observed by controlling the SMSI effect. Ethylene selectivity improved dramatically over Pd/α-Fe_2O_3-500H after Pd NPs being completely encapsulated (Fig. S12 in the ESM), much higher than Pd/α-Fe_2O_3 reduced at 200 (without encapsulation) and 400 °C (partial encapsulation of Pd NPs). The stability of Pd/α-Fe_2O_3-500H was tested at 130 °C, when acetylene conversion is increased from 97% to 100%, ethylene selectivity is decreased slightly and then stable because the conversion of alkene (reflected as alkene selectivity) is highly alkyne-coverage-dependent (Fig. S12(c) in the ESM). TGA result reveals that there is no obvious weight loss of the catalyst after durability test (Fig. S13 in the ESM), which means no side reactions of oligomerization or coking. Usually, C–C coupling of the reactant/intermediates needs at least four continuous Pd sites and coking generally is produced on extensive terrace sites [24, 74]. AC-STEM images of used Pd/α-Fe_2O_3-500H reveal the encapsulation layer is intact and no sintering of Pd single atoms or Pd NPs (Fig. S14 in the ESM), illuminating good catalyst stability.

4 Conclusions

In summary, we employed a simple encapsulation strategy to construct Pd SACs, improving ethylene selectivity dramatically in semi-hydrogenation of acetylene for Pd-based catalysts. Detailed characterization analysis suggested that Pd NPs would be completely encapsulated while the single Pd atoms exposed by high-temperature reduction based on the different SMSI occurrence conditions. Highly efficient and stable Pd_1/CeO_2 was successfully obtained, which showed the full acetylene conversion at 160 °C and the selectivity enhanced much to 85%. The strategy is universal and can be extended to other reducible oxide supported Pd catalysts, such as Pd_1/α-Fe_2O_3. This research provides an alternative approach to prepare stable Pd SACs with high selectivity for hydrogenation reaction.

Acknowledgements

This work was financially supported by the National Natural Science Foundation of China (Nos. 21972135, 21961142006, and 51701201), CAS Project for Young Scientists in Basic Research (No. YSBR-022), and the National Key Research and Development Program of China (No. 2021YFA1500503).

Electronic Supplementary Material: Supplementary material (XRD patterns, further STEM-HAADF images, CO-DRIFTS and XPS, reaction data and TGA results) is available in the online version of this article at https://doi.org/10.1007/s12274-022-4376-5.

References

[1] Borodziński, A.; Bond, G. C. Selective hydrogenation of ethyne in ethene-rich streams on palladium catalysts. Part 1. Effect of changes to the catalyst during reaction. *Catal. Rev.* **2006**, *48*, 91–144.

[2] Borodziński, A.; Bond, G. C. Selective hydrogenation of ethyne in ethene-rich streams on palladium catalysts, Part 2: Steady-state kinetics and effects of palladium particle size, carbon monoxide, and promoters. *Catal. Rev.* **2008**, *50*, 379–469.

[3] García-Mota, M.; Gómez-Díaz, J.; Novell-Leruth, G.; Vargas-Fuentes, C.; Bellarosa, L.; Bridier, B.; Pérez-Ramírez, J.; López, N. A density functional theory study of the "mythic" lindlar hydrogenation catalyst. *Theor. Chem. Acc.* **2011**, *128*, 663–673.

[4] Teschner, D.; Borsodi, J.; Wootsch, A.; Revay, Z.; Havecker, M.; Knop-Gericke, A.; Jackson, S. D.; Schlogl, R. The roles of subsurface carbon and hydrogen in palladium-catalyzed alkyne hydrogenation. *Science* **2008**, *320*, 86–89.

[5] Albani, D.; Shahrokhi, M.; Chen, Z. P.; Mitchell, S.; Hauert, R.; López, N.; Pérez-Ramírez, J. Selective ensembles in supported palladium sulfide nanoparticles for alkyne semi-hydrogenation. *Nat. Commun.* **2018**, *9*, 2634.

[6] Zhou, H. R.; Yang, X. F.; Li, L.; Liu, X. Y.; Huang, Y. Q.; Pan, X. L.; Wang, A. Q.; Li, J.; Zhang, T. PdZn intermetallic nanostructure with Pd-Zn-Pd ensembles for highly active and chemoselective semi-

hydrogenation of acetylene. *ACS Catal.* **2016**, *6*, 1054–1061.
[7] Feng, Q. C.; Zhao, S.; Wang, Y.; Dong, J. C.; Chen, W. X.; He, D. S.; Wang, D. S.; Yang, J.; Zhu, Y. M.; Zhu, H. L. et al. Isolated single-atom Pd sites in intermetallic nanostructures: High catalytic selectivity for semihydrogenation of alkynes. *J. Am. Chem. Soc.* **2017**, *139*, 7294–7301.
[8] Shao, L. D.; Zhang, W.; Armbrüster, M.; Teschner, D.; Girgsdies, F.; Zhang, B. S.; Timpe, O.; Friedrich, M.; Schlögl, R.; Su, D. S. Nanosizing intermetallic compounds onto carbon nanotubes: Active and selective hydrogenation catalysts. *Angew. Chem., Int. Ed.* **2011**, *50*, 10231–10235.
[9] Kyriakou, G.; Boucher, M. B.; Jewell, A. D.; Lewis, E. A.; Lawton, T. J.; Baber, A. E.; Tierney, H. L.; Flytzani-Stephanopoulos, M.; Sykes, E. C. H. Isolated metal atom geometries as a strategy for selective heterogeneous hydrogenations. *Science* **2012**, *335*, 1209–1212.
[10] Pei, G. X.; Liu, X. Y.; Wang, A. Q.; Lee, A. F.; Isaacs, M. A.; Li, L.; Pan, X. L.; Yang, X. F.; Wang, X. D.; Tai, Z. J. et al. Ag alloyed Pd single-atom catalysts for efficient selective hydrogenation of acetylene to ethylene in excess ethylene. *ACS Catal.* **2015**, *5*, 3717–3725.
[11] Pei, G. X.; Liu, X. Y.; Wang, A. Q.; Li, L.; Huang, Y. Q.; Zhang, T.; Lee, J. W.; Jang, B. W. L.; Mou, C. Y. Promotional effect of Pd single atoms on Au nanoparticles supported on silica for the selective hydrogenation of acetylene in excess ethylene. *New J. Chem.* **2014**, *38*, 2043–2051.
[12] Pei, G. X.; Liu, X. Y.; Yang, X. F.; Zhang, L. L.; Wang, A. Q.; Li, L.; Wang, H.; Wang, X. D.; Zhang, T. Performance of Cu-alloyed Pd single-atom catalyst for semihydrogenation of acetylene under simulated front-end conditions. *ACS Catal.* **2017**, *7*, 1491–1500.
[13] Kovnir, K.; Armbrüster, M.; Teschner, D.; Venkov, T. V.; Szentmiklósi, L.; Jentoft, F. C.; Knop-Gericke, A.; Grin, Y.; Schlögl, R. *In situ* surface characterization of the intermetallic compound PdGa—A highly selective hydrogenation catalyst. *Surf. Sci.* **2009**, *603*, 1784–1792.
[14] Li, X. T.; Chen, L.; Shang, C.; Liu, Z. P. *In situ* surface structures of PdAg catalyst and their influence on acetylene semihydrogenation revealed by machine learning and experiment. *J. Am. Chem. Soc.* **2021**, *143*, 6281–6292.
[15] Zheng, W. J.; Wang, Y.; Wang, B. J.; Fan, M. H.; Ling, L. X.; Zhang, R. G. C_2H_2 selective hydrogenation to C_2H_4: Engineering the surface structure of Pd-based alloy catalysts to adjust the catalytic performance. *J. Phys. Chem. C* **2021**, *125*, 15251–15261.
[16] Kim, S. K.; Lee, J. H.; Ahn, I. Y.; Kim, W. J.; Moon, S. H. Performance of Cu-promoted Pd catalysts prepared by adding Cu using a surface redox method in acetylene hydrogenation. *App. Catal. A Gen.* **2011**, *401*, 12–19.
[17] Lang, R.; Du, X. R.; Huang, Y. K.; Jiang, X. Z.; Zhang, Q.; Guo, Y. L.; Liu, K. P.; Qiao, B. T.; Wang, A. Q.; Zhang, T. Single-atom catalysts based on the metal−oxide interaction. *Chem. Rev.* **2020**, *120*, 11986–12043.
[18] Qiao, B. T.; Wang, A. Q.; Yang, X. F.; Allard, L. F.; Jiang, Z.; Cui, Y. T.; Liu, J. Y.; Li, J.; Zhang, T. Single-atom catalysis of CO oxidation using Pt_1/FeO_x. *Nat. Chem.* **2011**, *3*, 634–641.
[19] Wang, X.; Zhang, Y. W.; Wu, J.; Zhang, Z.; Liao, Q. L.; Kang, Z.; Zhang, Y. Single-atom engineering to ignite 2D transition metal dichalcogenide based catalysis: Fundamentals, progress, and beyond. *Chem. Rev.* **2022**, *122*, 1273–1348.
[20] Wei, Y. S.; Zhang, M.; Zou, R. Q.; Xu, Q. Metal-organic framework-based catalysts with single metal sites. *Chem. Rev.* **2020**, *120*, 12089–12174.
[21] Wang, Y. X.; Su, H. Y.; He, Y. H.; Li, L. G.; Zhu, S. Q.; Shen, H.; Xie, P. F.; Fu, X. B.; Zhou, G. Y.; Feng, C. et al. Advanced electrocatalysts with single-metal-atom active sites. *Chem. Rev.* **2020**, *120*, 12217–12314.
[22] Li, Z. J.; Wang, D. H.; Wu, Y. E.; Li, Y. D. Recent advances in the precise control of isolated single-site catalysts by chemical methods. *Natl. Sci. Rev.* **2018**, *5*, 673–689.
[23] Zhou, X. M. TiO_2-supported single-atom catalysts for photocatalytic reactions. *Acta Phys. Chim. Sin.* **2021**, *37*, 2008064.
[24] Zhang, L. L.; Zhou, M. X.; Wang, A. Q.; Zhang, T. Selective hydrogenation over supported metal catalysts: From nanoparticles to single atoms. *Chem. Rev.* **2020**, *120*, 683–733.
[25] Liu, Y. W.; Wang, B. X.; Fu, Q.; Liu, W.; Wang, Y.; Gu, L.; Wang, D. S.; Li, Y. D. Polyoxometalate-based metal-organic framework as molecular sieve for highly selective semi-hydrogenation of acetylene on isolated single Pd atom sites. *Angew. Chem., Int. Ed.* **2021**, *60*, 22522–22528.
[26] Liu, P. X.; Zhao, Y.; Qin, R. X.; Mo, S. G.; Chen, G. X.; Gu, L.; Chevrier, D. M.; Zhang, P.; Guo, Q.; Zang, D. D. et al. Photochemical route for synthesizing atomically dispersed palladium catalysts. *Science* **2016**, *352*, 797–800.
[27] Wei, S. J.; Li, A.; Liu, J. C.; Li, Z.; Chen, W. X.; Gong, Y.; Zhang, Q. H.; Cheong, W. C.; Wang, Y.; Zheng, L. R. et al. Direct observation of noble metal nanoparticles transforming to thermally stable single atoms. *Nat. Nanotechnol.* **2018**, *13*, 856–861.
[28] Ge, X. X.; Zhou, P.; Zhang, Q. H.; Xia, Z. H.; Chen, S. L.; Gao, P.; Zhang, Z.; Gu, L.; Guo, S. J. Palladium single atoms on TiO_2 as a photocatalytic sensing platform for analyzing the organophosphorus pesticide chlorpyrifos. *Angew. Chem., Int. Ed.* **2020**, *59*, 232–236.
[29] Xu, H. D.; Zhang, Z. H.; Liu, J. X.; Do-Thanh, C. L.; Chen, H.; Xu, S. H.; Lin, Q. J.; Jiao, Y.; Wang, J. L.; Wang, Y. et al. Entropy-stabilized single-atom Pd catalysts via high-entropy fluorite oxide supports. *Nat. Commun.* **2020**, *11*, 3908.
[30] Tauster, S. J.; Fung, S. C. Strong metal–support interactions: Occurrence among the binary oxides of groups IIA-VB. *J. Catal.* **1978**, *55*, 29–35.
[31] Tauster, S. J.; Fung, S. C.; Garten, R. L. Strong metal–support interactions. Group 8 noble metals supported on titanium dioxide. *J. Am. Chem. Soc.* **1978**, *100*, 170–175.
[32] Tauster, S. J. Strong metal–support interactions. *Acc. Chem. Res.* **1987**, *20*, 389–394.
[33] Bernal, S.; Calvino, J. J.; Cauqui, M. A.; Gatica, J. M.; Cartes, C. L.; Omil, J. A. P.; Pintado, J. M. Some contributions of electron microscopy to the characterisation of the strong metal–support interaction effect. *Catal. Today* **2003**, *77*, 385–406.
[34] Naito, S.; Aida, S.; Kasahara, T.; Miyao, T. Infrared spectroscopic study on the reaction mechanism of CO hydrogenation over Pd/CeO_2. *Res. Chem. Intermed.* **2006**, *32*, 279–290.
[35] d'Alnoncourt, R. N.; Friedrich, M.; Kunkes, E.; Rosenthal, D.; Girgsdies, F.; Zhang, B. S.; Shao, L. D.; Schuster, M.; Behrens, M.; Schlögl, R. Strong metal–support interactions between palladium and iron oxide and their effect on CO oxidation. *J. Catal.* **2014**, *317*, 220–228.
[36] Bernal. S.; Botana. F. J.; Calvino. J. J.; Cifredo. G. A.; Pe´rez-Omil, J. A.; Pintado. J. M. HREM study of the behaviour of a Rh/CeO_2 catalyst under high temperature reducing and oxidizing conditions. *Catal. Today* **1995**, *23*, 219–250.
[37] Kast, P.; Friedrich, M.; Teschner, D.; Girgsdies, F.; Lunkenbein, T.; d'Alnoncourt, R. N.; Behrens, M.; Schlögl, R. CO oxidation as a test reaction for strong metal–support interaction in nanostructured Pd/FeO powder catalysts. *Appl. Catal. A Gen.* **2015**, *502*, 8–17.
[38] Tauster, S. J.; Fung, S. C.; Baker, R. T. K.; Horsley, J. A. Strong interactions in supported-metal catalysts. *Science* **1981**, *211*, 1121–1125.
[39] Liu, X. Y.; Liu, M. H.; Luo, Y. C.; Mou, C. Y.; Lin, S. D.; Cheng, H. K.; Chen, J. M.; Lee, J. F.; Lin, T. S. Strong metal–support interactions between gold nanoparticles and ZnO nanorods in CO oxidation. *J. Am. Chem. Soc.* **2012**, *134*, 10251–10258.
[40] Qiao, B. T.; Liang, J. X.; Wang, A. Q.; Xu, C. Q.; Li, J.; Zhang, T.; Liu, J. J. Ultrastable single-atom gold catalysts with strong covalent metal–support interaction (CMSI). *Nano Res.* **2015**, *8*, 2913–2924.
[41] Hu, P. P.; Huang, Z. W.; Amghouz, Z.; Makkee, M.; Xu, F.; Kapteijn, F.; Dikhtiarenko, A.; Chen, Y. X.; Gu, X.; Tang, X. F. Electronic metal–support interactions in single-atom catalysts. *Angew. Chem., Int. Ed.* **2014**, *53*, 3418–3421.
[42] Bruix, A.; Rodriguez, J. A.; Ramírez, P. J.; Senanayake, S. D.; Evans, J.; Park, J. B.; Stacchiola, D.; Liu, P.; Hrbek, J.; Illas, F. A new type of strong metal–support interaction and the production of H_2 through the transformation of water on $Pt/CeO_2(111)$ and

Pt/CeO_x/TiO_2(110) catalysts. *J. Am. Chem. Soc.* **2012**, *134*, 8968–8974.

[43] Du, X. R.; Huang, Y. K.; Pan, X. L.; Han, B.; Su, Y.; Jiang, Q. K.; Li, M. R.; Tang, H. L.; Li, G.; Qiao, B. T. Size-dependent strong metal–support interaction in TiO_2 supported Au nanocatalysts. *Nat. Commun.* **2020**, *11*, 5811.

[44] Ma, D. Size-dependent strong metal–support interaction. *Acta Phys. Chim. Sin.* **2022**, *38*, 2101039.

[45] Wang, H.; Wang, L.; Lin, D.; Feng, X.; Niu, Y. M.; Zhang, B. S.; Xiao, F. S. Strong metal–support interactions on gold nanoparticle catalysts achieved through Le chatelier's principle. *Nat. Catal.* **2021**, *4*, 418–424.

[46] Zhang, Y. S.; Liu, J. X.; Qian, K.; Jia, A. P.; Li, D.; Shi, L.; Hu, J.; Zhu, J. F.; Huang, W. X. Structure sensitivity of Au-TiO_2 strong metal–support interactions. *Angew. Chem., Int. Ed.* **2021**, *60*, 12074–12081.

[47] Tang, H. L.; Liu, F.; Wei, J. K.; Qiao, B. T.; Zhao, K. F.; Su, Y.; Jin, C. Z.; Li, L.; Liu, J. Y.; Wang, J. H. et al. Ultrastable hydroxyapatite/titanium-dioxide-supported gold nanocatalyst with strong metal–support interaction for carbon monoxide oxidation. *Angew. Chem., Int. Ed.* **2016**, *55*, 10606–10611.

[48] Yang, J. R. ; Li, W. H. ; Tan, S. D. ; Xu, K. N. ; Wang, Y. ; Wang, D. S. ; Li, Y. D. The electronic metal–support interaction directing the design of single atomic site catalysts: Achieving high efficiency towards hydrogen evolution. *Angew. Chem., Int. Ed.* **2012**, *60*, 19085–19091.

[49] Dong, J. H.; Fu, Q.; Li, H. B.; Xiao, J. P.; Yang, B.; Zhang, B. S.; Bai, Y. X.; Song, T. Y.; Zhang, R. K.; Gao, L. J. et al. Reaction-induced strong metal–support interactions between metals and inert boron nitride nanosheets. *J. Am. Chem. Soc.* **2020**, *142*, 17167–17174.

[50] Li, W. H.; Yang, J. R.; Jing, H. Y.; Zhang, J.; Wang, Y.; Li, J.; Zhao, J.; Wang, D. S.; Li, Y. D. Creating high regioselectivity by electronic metal–support interaction of a single-atomic-site catalyst. *J. Am. Chem. Soc.* **2021**, *143*, 15453–15461.

[51] Han, B.; Guo, Y. L.; Huang, Y. K.; Xi, W.; Xu, J.; Luo, J.; Qi, H. F.; Ren, Y. J.; Liu, X. Y.; Qiao, B. T. et al. Strong metal–support interactions between Pt single atoms and TiO_2. *Angew. Chem., Int. Ed.* **2020**, *59*, 11824–11829.

[52] Chen, F.; Li, T. B.; Pan, X. L.; Guo, Y. L.; Han, B.; Liu, F.; Qiao, B. T.; Wang, A. Q.; Zhang, T. Pd_1/CeO_2 single-atom catalyst for alkoxycarbonylation of aryl iodides. *Sci. China Mater.* **2020**, *63*, 959–964.

[53] Spezzati, G.; Su, Y. Q.; Hofmann, J. P.; Benavidez, A. D.; DeLaRiva, A. T.; McCabe, J.; Datye, A. K.; Hensen, E. J. M. Atomically dispersed Pd-O species on CeO_2(111) as highly active sites for low-temperature CO oxidation. *ACS Catal.* **2017**, *7*, 6887–6891.

[54] Lou, Y.; Jiang, F.; Zhu, W.; Wang, L.; Yao, T. Y.; Wang, S. S.; Yang, B.; Yang, B.; Zhu, Y. F.; Liu, X. H. CeO_2 supported Pd dimers boosting CO_2 hydrogenation to ethanol. *Appl. Catal. B Environ.* **2021**, *291*, 120122.

[55] Haller, G. L.; Resasco, D. E. Metal–support interaction: Group VIII metals and reducible oxides. *Adv. Catal.* **1989**, *36*, 173–235.

[56] Binet, C.; Jadi, A.; Lavalley, J. C.; Boutonnet-Kizling, M. Metal support interaction in Pd/CeO_2 catalysts: Fourier-transform infrared studies of the effects of the reduction temperature and metal loading. Part 1.-Catalysts prepared by the microemulsion technique. *J. Chem. Soc. Faraday Trans.* **1992**, *88*, 2079–2084.

[57] Trovarelli, A.; Dolcetti, G.; De Leitenburg, C.; Kašpar, J.; Finetti, P.; Santoni, A. Rh–CeO_2 Interaction induced by high-temperature reduction. Characterization and catalytic behaviour in transient and continuous conditions. *J. Chem. Soc. Faraday Trans.* **1992**, *88*, 1311–1319.

[58] Aitbekova, A.; Wu, L. H.; Wrasman, C. J.; Boubnov, A.; Hoffman, A. S.; Goodman, E. D.; Bare, S. R.; Cargnello, M. Low-temperature restructuring of CeO_2-supported Ru nanoparticles determines selectivity in CO_2 catalytic reduction. *J. Am. Chem. Soc.* **2018**, *140*, 13736–13745.

[59] Jones, J.; Xiong, H. F.; DeLaRiva, A. T.; Peterson, E. J.; Pham, H.; Challa, S. R.; Qi, G.; Oh, S.; Wiebenga, M. H.; Hernández, X. I. P. et al. Thermally stable single-atom platinum-on-ceria catalysts via atom trapping. *Science* **2016**, *353*, 150–154.

[60] Newton, M. A.; Belver-Coldeira, C.; Martínez-Arias, A.; Fernández-García, M. "Oxidationless" promotion of rapid palladium redispersion by oxygen during redox CO/(NO+O_2) cycling. *Angew. Chem., Int. Ed.* **2007**, *46*, 8629–8631.

[61] Jeong, H.; Bae, J.; Han, J. W.; Lee, H. Promoting effects of hydrothermal treatment on the activity and durability of Pd/CeO_2 catalysts for CO oxidation. *ACS Catal.* **2017**, *7*, 7097–7105.

[62] Xin, P. Y.; Li, J.; Xiong, Y.; Wu, X.; Dong, J. C.; Chen, W. X.; Wang, Y.; Gu, L.; Luo, J.; Rong, H. P. et al. Revealing the active species for aerobic alcohol oxidation by using uniform supported palladium catalysts. *Angew. Chem., Int. Ed.* **2018**, *57*, 4642–4646.

[63] Ma, J.; Lou, Y.; Cai, Y. F.; Zhao, Z. Y.; Wang, L.; Zhan, W. C.; Guo, Y. L.; Guo, Y. The relationship between the chemical state of Pd species and the catalytic activity for methane combustion on Pd/CeO_2. *Catal. Sci. Technol.* **2018**, *8*, 2567–2577.

[64] Chen, Y. X.; Chen, J. X.; Qu, W. Y.; George, C.; Aouine, M.; Vernoux, P.; Tang, X. F. Well-defined palladium–ceria interfacial electronic effects trigger CO oxidation. *Chem. Commun.* **2018**, *54*, 10140–10143.

[65] Boronin, A. I.; Slavinskaya, E. M.; Danilova, I. G.; Gulyaev, R. V.; Amosov, Y. I.; Kuznetsov, P. A.; Polukhina, I. A.; Koscheev, S. V.; Zaikovskii, V. I.; Noskov, A. S. Investigation of palladium interaction with cerium oxide and its state in catalysts for low-temperature CO oxidation. *Catal. Today* **2009**, *144*, 201–211.

[66] Gulyaev, R. V. ; Stadnichenko, A. I. ; Slavinskaya, E. M. ; Ivanova, A. S. ; Koscheev, S. V. ; Boronin, A. I. *In situ* preparation and investigation of Pd/CeO_2 catalysts for the low-temperature oxidation of CO. *Appl. Catal. A Gen.* **2012**, *439–440*, 41–50.

[67] Zhang, Y. H.; Cai, Y. F.; Guo, Y.; Wang, H. F.; Wang, L.; Lou, Y.; Guo, Y. L.; Lu, G. Z.; Wang, Y. Q. The effects of the Pd chemical state on the activity of Pd/Al_2O_3 catalysts in CO oxidation. *Catal. Sci. Technol.* **2014**, *4*, 3973–3980.

[68] Luo, Y.; Villaseca, S. A.; Friedrich, M.; Teschner, D.; Knop-Gericke, A.; Armbrüster, M. Addressing electronic effects in the semi-hydrogenation of ethyne by in Pd_2 and intermetallic Ga-Pd compounds. *J. Catal.* **2016**, *338*, 265–272.

[69] Huang, F.; Deng, Y. C.; Chen, Y. L.; Cai, X. B.; Peng, M.; Jia, Z. M.; Ren, P. J.; Xiao, D. Q.; Wen, X. D.; Wang, N. et al. Atomically dispersed Pd on nanodiamond/graphene hybrid for selective hydrogenation of acetylene. *J. Am. Chem. Soc.* **2018**, *140*, 13142–13146.

[70] Armbrüster, M.; Kovnir, K.; Behrens, M.; Teschner, D.; Grin, Y.; Schlögl, R. Pd-Ga intermetallic compounds as highly selective semihydrogenation catalysts. *J. Am. Chem. Soc.* **2010**, *132*, 14745–14747.

[71] Armbrüster, M.; Wowsnick, G.; Friedrich, M.; Heggen, M.; Cardoso-Gil, R. Synthesis and catalytic properties of nanoparticulate intermetallic Ga-Pd compounds. *J. Am. Chem. Soc.* **2011**, *133*, 9112–9118.

[72] Vilé, G.; Bridier, B.; Wichert, J.; Pérez-Ramírez, J. Ceria in hydrogenation catalysis: High selectivity in the conversion of alkynes to olefins. *Angew. Chem., Int. Ed.* **2012**, *51*, 8620–8623.

[73] Haller, G. L. New catalytic concepts from new materials: Understanding catalysis from a fundamental perspective, past, present, and future. *J. Catal.* **2003**, *216*, 12–22.

[74] Vignola, E.; Steinmann, S. N.; Al Farra, A.; Vandegehuchte, B. D.; Curulla, D.; Sautet, P. Evaluating the risk of C–C bond formation during selective hydrogenation of acetylene on palladium. *ACS Catal.* **2018**, *8*, 1662–1671.